Spring 5-19-2017

Computational Fluid Dynamics Modeling and Simulations of Fast Fluidized Bed and Moving Bed Reactors for Chemical Looping Combustion

Mengqiao Yang
Washington University in St. Louis

WASHINGTON UNIVERSITY IN ST. LOUIS

School of Engineering & Applied Science

Department of Mechanical Engineering and Materials Science

Thesis Examination Committee:
Dr. Ramesh K. Agarwal, Chair
Dr. Swami Karunamoorthy
Dr. Qiulin Qu

Computational Fluid Dynamics Modeling and Simulations of Fast Fluidized Bed and Moving Bed Reactors for Chemical Looping Combustion

by
Mengqiao Yang

A thesis presented to
the School of Engineering and Applied Science
of Washington University in
partial fulfillment of the
requirements for the degree
of Master of Science

May 2017
St. Louis, Missouri

Table of Contents

List of Figures iii
List of Tables v
Acknowledgments vi
Abstract viii
Chapter 1: Introduction 1
Chapter 2: Transient Cold Flow Simulation of a Fast Fluidized Bed in a Fuel Reactor 7
2.1 Modeling Approach for DDPM Simulation 7
2.2 Simulation of a Fast Fluidized Bed with Molochite as Bed Material 9
2.3 Simulation of a Fast Fluidized Bed with FE100 as Bed Material 18
2.4 Conclusion 26
Chapter 3: Transient Cold Flow Simulation of a Moving Bed in an Air Reactor 28
3.1 Modeling Approach for DEM Simulation 28
3.2 Simulation of Cross Flow Moving Fluidized Bed with Iron as Bed Material 30
3.2.1 Geometry and Mesh 30
3.2.2 Modeling Parameters 32
3.2.3 Results and Analysis 33
3.2.4 Conclusion 39
Chapter 4: Conclusion and Future Work 40

List of Figures

Figure 1: Eighty Percent Increase in Worldwide Fossil Fuel Consumption from 1980 to 2012.... 2
Figure 2: Schematic of the CLC process 3
Figure 3: Geldart's Powder Classification Diagram for Fluidization 4
Figure 4: Geometry outline and mesh (in upper and low part) of the fuel reactor of Haider et al. [17] 10
Figure 5: Particle tracks colored by velocity magnitude for the fast fluidized bed simulation with molochite 13
Figure 6: Time variation of outlet mass flow rate for the fast fluidized bed simulation with molochite 14
Figure 7: Time variation of static pressure at various heights for the fast fluidized bed simulation with molochite 15
Figure 8: Time variation of volume fraction at various heights for the fast fluidized bed simulation with molochite 16
Figure 9: Comparison of pressure variation at various heights for the fast fluidized bed simulation with molochite 17
Figure 10: Comparison of volume fraction at various heights for the fast fluidized bed simulation with molochite 18
Figure 11: Particles tracks colored by velocity magnitude for the fast fluidized bed simulation with FE100 21
Figure 12: Time variation of outlet mass flow rate for the fast fluidized bed simulation with FE100 22
Figure 13: Time variation of static pressure at various heights for the fast fluidized bed simulation with FE100 24
Figure 14: Time variation of volume fraction at various heights for the fast fluidized bed simulation with FE100 24
Figure 15: Comparison of pressure variation at various heights for the fast fluidized bed simulation with FE100 25
Figure 16: Comparison of volume fraction at various heights for the fast fluidized bed simulation with FE100 26
Figure 17: Schematic of particle collision model for DEM 29
Figure 18: Geometry outline of the air reactor of Wang et al. [24] 31
Figure 19: Mesh (in upper and lower part) of the air reactor of Wang et al. [24] 31
Figure 20： Particle tracks colored by velocity magnitude for the moving bed simulation with iron 34
Figure 21: Time variation of total pressure for the moving bed simulation with iron 35
Figure 22: Time variation of particle velocity at various heights for the moving bed simulation with iron 36

Figure 23: Fully developed particle velocity distribution at various heights for the moving bed simulation with iron 37
Figure 24: Developing flow field streamlines for the moving bed simulation with iron 38

List of Tables

Table 1: Key modeling parameters for fast fluidized bed simulation with molochite as bed material 11
Table 2: Key modeling parameters for fast fluidized bed simulation with FE100 as bed material 19
Table 3: Key modeling parameters for moving bed simulation with iron as bed material..... 33

Acknowledgments

I would like to express my gratitude to my academic and research advisor, Dr. Ramesh Agarwal, for his continuous encouragement and limitless patience during my master's studies. Under his instructions, I have learned not only how to do research but also the method for systematically solving the scientific problems and exploring new science.

I would also like to thank Dr. Swami Karunamoorthy and Dr. Qiulin Qu for taking the time to serve on my thesis defense committee.

I would also like to express my appreciation to all my colleagues working in Computational Fluid Dynamics Laboratory for their encouragement and company. I want to especially thank Dr. Subhodeep Banerjee for his advice and guidance during this research.

I especially want to thank my parents for constant encouragement and affection. Without the ceaseless support from my parents, I would not have any chance to study abroad and experience a different life.

Mengqiao Yang

Washington University in St. Louis

May 2017

Dedicated to my parents.

ABSTRACT OF THE THESIS

Computational Fluid Dynamics Modeling and Simulations of Fast Fluidized Bed and Moving Bed Reactors for Chemical Looping Combustion

by

Mengqiao Yang

Master of Science in Mechanical Engineering

Department of Mechanical Engineering and Materials Science

Washington University in St. Louis, 2017

Research Advisor: Dr. Ramesh K. Agarwal

Chemical-looping combustion (CLC) is a next generation carbon capture technology with high efficiency and low cost. To assess the potential of this technology for industrial scale power plants, thousands of laboratory scale and many pilot-scale plants have been designed and tested. In recent years, to obtain a thorough understanding of the hydrodynamic behavior inside the reactors and chemical looping combustion process, high-fidelity numerical simulation using Computational Fluid Dynamics(CFD) have been performed. However, CFD simulations in the literature have been limited reported compared to the laboratory scale experiments.

In this thesis, cold flow simulations of a CLC fuel reactor are performed corresponding to the pilot-scale experiment of a dual fluidized bed CLC system. By employing the dense discrete phase model (DDPM) with hydrodynamics, the fluidization behavior is captured in the simulations, which also shows stable circulation in the reactor. Comparisons of captured static pressures and volume fractions in the reactor show excellent agreement with the experimental data. To further

verify this computational model, different bed materials are employed in the simulations and again satisfactory results are obtained.

In a second project, cold flow simulations of a cross-flow moving bed in an air reactor are performed corresponding to a laboratory-scale experiment. Because of the requirement of high accuracy in these simulations, discrete element method (DEM) is employed. The simulation results for the particle behavior and pressure drop are in satisfactory agreement with the experiment. Time varied particle velocity distributions are obtained and a dual-vortex formation is observed. Again, simulations achieved stable circulation inside the reactor. This work has provided important insight into controlling the pressure gradient and recirculation in the moving bed reactor.

Chapter 1: Introduction

In 1896, Arrhenius was the first to quantify the contribution of CO_2 to the greenhouse effect and analyze the relationship between long-term variations in climate and the concentration of CO_2 [1]. Since 1970s, fossil fuels have overwhelmingly been the fuel of choice—today the world uses 39 per cent more oil, 107 per cent more coal, and 131 per cent more natural gas than it did in 1980 [2]. Greenhouse gases such as CO_2 produced from burning fossil fuels absorbs infrared thermal radiation from solar energy and results in an increase in the atmospheric temperature causing global warming. The resulting changes in rain patterns, melting of polar ice caps and rising sea levels will sharply affect human beings, animals, and ecosystems. Although renewable energy sources such as solar, wind, geothermal and nuclear can help reduce the fossil fuel consumption, their relative range in the near future will remain limited due to their high cost and low efficiency. Since fossil fuels are likely to remain their position as the dominant energy source in the near future as shown in Figure 1 [3], developing techniques for carbon capture from power plants has become the focus of modern combustion technology research in recent years.

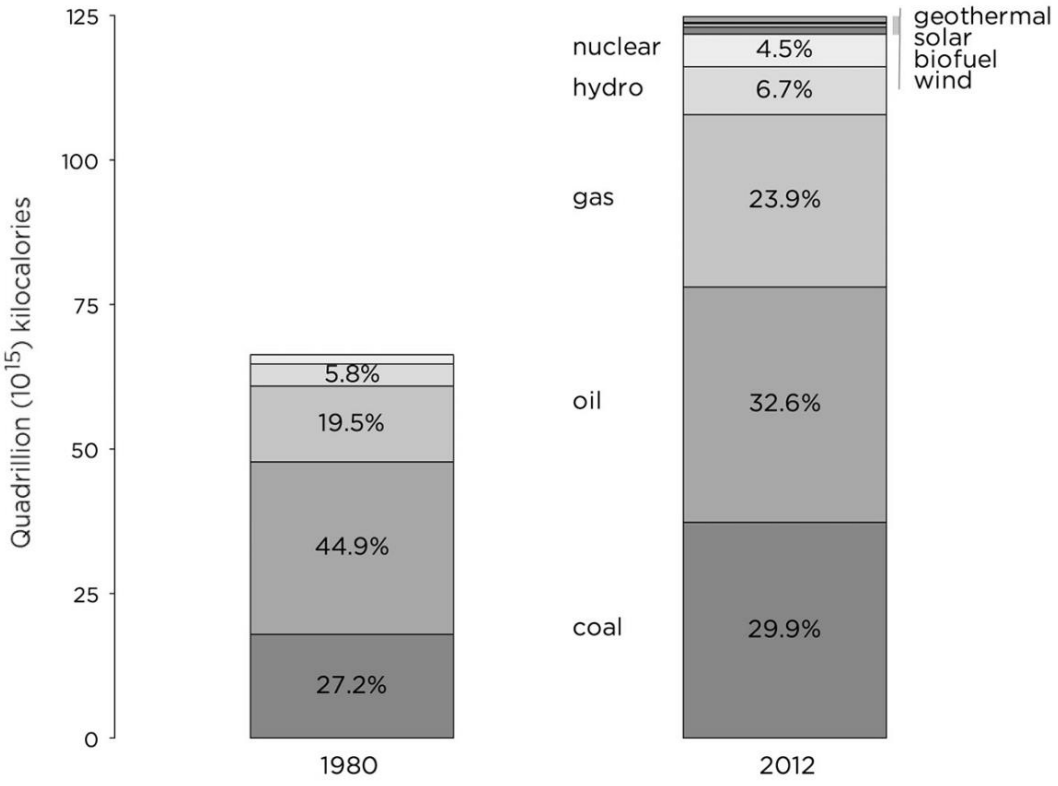

Figure 1: Eighty Percent Increase in Worldwide Fossil Fuel Consumption from 1980 to 2012

One of these modern combustion techniques is the chemical looping combustion (CLC), which shows advantages of both the low cost and high efficiency. In order to avoid direct contact between the fuel and oxygen, this technology requires metal oxide particles as the oxygen carrier. Gaseous or solid fuel is injected into the fuel reactor where it reacts with the oxygen carrier, then the reduced oxygen carrier is sent to the air reactor, which is oxidized by air, and is finally transported back to the fuel reactor to complete the looping process as illustrated in Figure 2. In this process, CO_2 and H_2O produced in the fuel reactor are thus inherently separated from the air mixture and no extra separation process is required compared to the traditional carbon capture technologies such as post-combustion capture or oxy-fuel combustion, resulting in 12 to 20 percent increase in the energy efficiency [4].

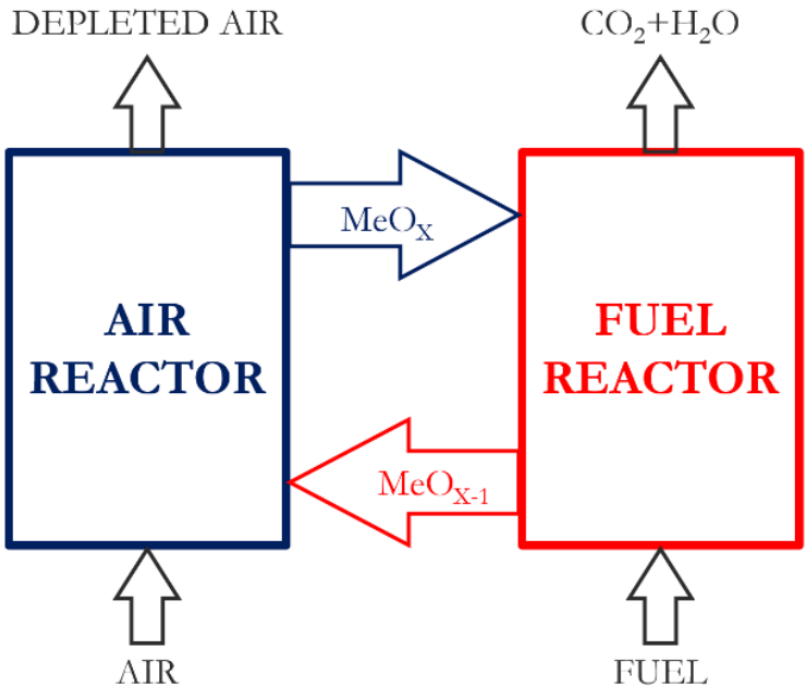

Figure 2: Schematic of the CLC process

The choice of oxygen carrier has a significant effect on the performance of a CLC system—the ideal oxygen carrier should have high conversion and reaction rates as well as nontoxic behavior [5]. The use of solid fuels, such as coal or biomass, has also attracted the attention of researchers and several injection methods have been put forward. One method is to inject coal into syngas and get a fully gasified fuel mixture which is subsequently injected into the fuel reactor [6]. From a CLC perspective, using pre-gasified coal in the fuel reactor is essentially identical to using gaseous fuel. An alternate method, known as coal-direct chemical looping combustion (CD-CLC), is to inject pulverized coal directly into fuel reactor where it devolatilizes and is gasified before reacting with the fuel [7]. In addition, the reactor configurations, such as packed or moving bed, bubbling bed, and fast fluidized bed, also have an influence on the system behavior. These fluidized bed configurations are determined by the particle size and velocity of the injection gas. Based on

diameter of the powder particles, Geldart has classified the powder into four groups, as shown in Figure 3 [8].

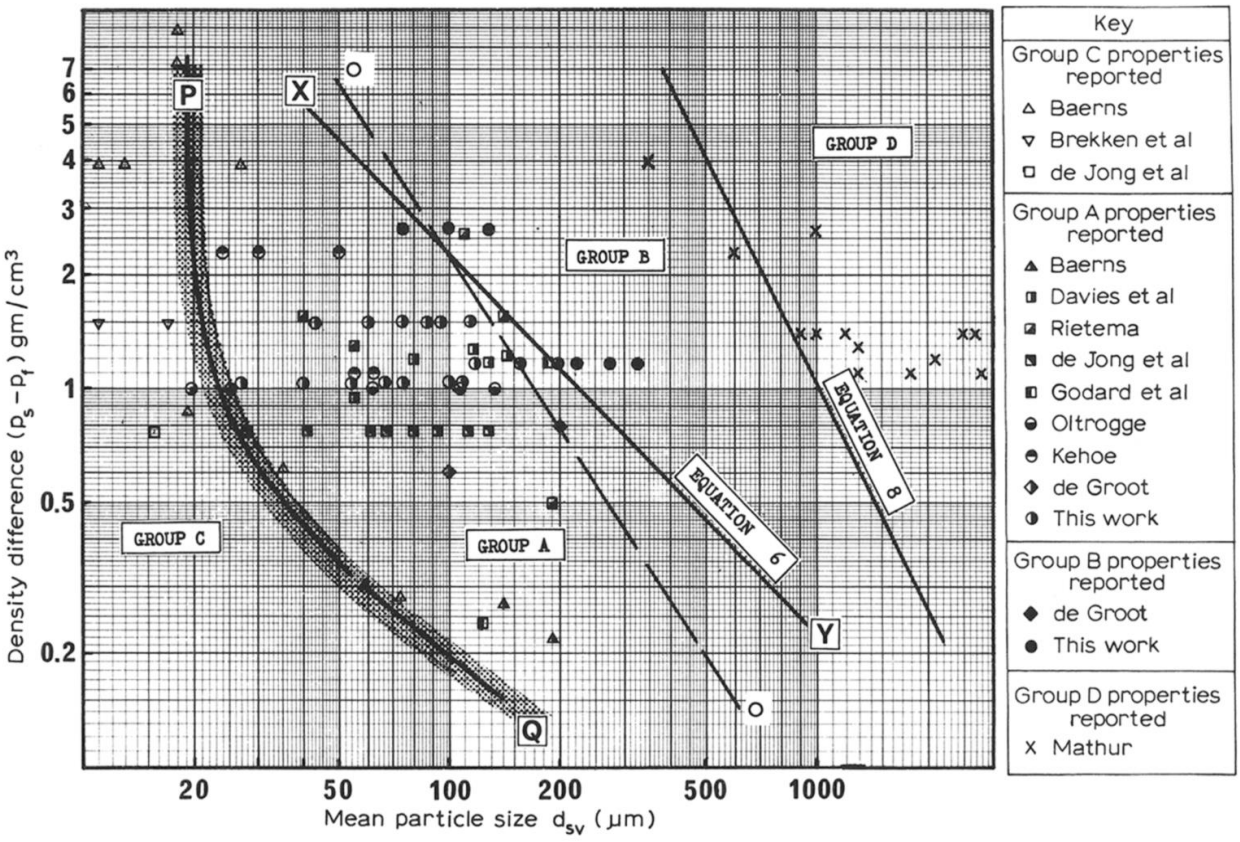

Figure 3: Geldart's Powder Classification Diagram for Fluidization

Due to the high cost associated with physical experiments of CLC systems as well as the rapid development of computer science and hardware, computational fluid dynamics (CFD) has provided a cheaper alternative for the study of CLC systems [9]. However, even though laboratory-scale and pilot-scale studies of CLC are common in the literature, numerical simulations using CFD have been limited. Currently, numerical approaches can be broadly categorized as Eulerian-Eulerian or Eulerian-Lagrangian. By selecting different modeling approach, simulations of multiphase flows of granular solid and gas systems can be conducted to meet the demand of different level accuracy. The Eulerian-Eulerian or Two-Fluid model considers both gas and solid

phase as interpenetrating continua, and the mass, momentum and energy equations are obtained by averaging the particle variables over an appropriate region with constitutive relations for the solid phase obtained from the kinetic theory of granular flow, which is an extension of classical kinetic gas theory. The work of Ding and Gidaspow [10] has shown good agreement with the experiment data for a bubbling bed simulation using the two-fluid model. The Eulerian-Eulerian approach requires less computational resources and is often employed for pilot and industrial scale modeling [11]. However, its disadvantage is also obvious: due to its treatment of the solid phase as a continuous phase, it can no longer trace the particles dynamic behavior. The Eulerian-Lagrangian approach, also known as discrete element method (DEM) treats the gas as a continuous phase and the solids as discrete particles that are tracked individually. The particle tracking is coupled with CFD solution for the fluid phase by considering the interaction between the particles and the fluid separately for each particle, so that particles conditions at different position and different time can be tracked. However, due to the limitation of computational resources, DEM models are typically limited to small scale applications and the number of particles are generally constrained to around 10^6 [12]. To avoid this limitation, the dense discrete phase model (DDPM) has been put forward [13]. DDPM no longer explicitly tracks the details of particle-particle and particle-wall collisions but uses a force to represent the details of the collisions, which allows the simulations to be less compute intensive. Since DDPM can implement the realistic particle distribution and track the discrete nature while maintaining a lower computational cost than DEM [14], it is a good modeling approach for simulation of a pilot-scale project. To further enhance the efficiency of simulation process, parcel concept has also been put forward. Parcels are statistical representations of a cluster of particles, and each parcel stands for either a fraction of the total continuous mass flow rate or the total mass flow released in a time step [15].

In addition, due to the limitations of reactor configurations and operations, it is impossible to accurately control the solid transfer and circulation rates as well as the heat transfer rate. Therefore, a cold flow model is generally employed to understand the hydrodynamic behavior inside the bed.

This thesis consists of two basic cold flow simulations of chemical looping combustion. The first simulation is to simulate a fast fluidized bed in a dual circulating system by employing the dense discrete phase model, two simulations are conducted using two different bed materials to investigate the influence of bed material. The second simulation employs the discrete element method to simulate a cross flow moving bed corresponding to a laboratory-scale experiment. In both cases, stable circulation is achieved and hydrodynamic behavior of particles is analyzed.

Chapter 2: Transient Cold Flow Simulation of a Fast Fluidized Bed in a Fuel Reactor

In this chapter, the methodology for simulating a fast fluidized bed in a fuel reactor is to use Computational Fluid Dynamics (CFD) software, ANSYS Fluent, release version 14.5. Due to the need of tracing the particles' trajectories and due to relatively large number of particles, dense discrete phase model (DDPM) is adopted in the simulations. In ANSYS Fluent, the dense discrete phase formulation assumes that the solid phase is sufficiently dilute so that the particle-particle interaction and the effects of the particle volume fraction on the gas phase can be neglected; the volume fraction of the solid phase should be constrained within 12 percent. Since no chemical reactions are considered, only the mass and momentum conservation equations are required to compute the gas phase flow field.

2.1 Modeling Approach for DDPM Simulation

The gas phase is treated as a continuous phase and the mass conservation (continuity) equation can be expressed as

$$\frac{\partial}{\partial t}(\alpha_f \rho_f) + \nabla \cdot (\alpha_f \rho_f \boldsymbol{u}_f) = 0 \qquad (1)$$

where α_f, ρ_f and $\boldsymbol{u}_f$ represent the local volume fraction, density, and velocity of the fluid phase respectively. The conversation of momentum equation can be written as

$$\frac{\partial}{\partial t}(\alpha_f \rho_f \boldsymbol{u}_f) + \nabla \cdot (\alpha_f \rho_f \boldsymbol{u}_f \boldsymbol{u}_f) = -\alpha_f \nabla p_f - \nabla \cdot \bar{\bar{\tau}}_f + \alpha_f \rho_f \mathbf{g} - \boldsymbol{R}_{\text{sg}} \qquad (2)$$

where p_f, $\bar{\bar{\tau}}_f$, and **g** represent the fluid pressure, the fluid shear stress tensor, and the acceleration due to gravity respectively, and $\boldsymbol{R}_{sg}$ is the transfer of fluid momentum to the solid phase obtained from the average of the drag forces acting on all the discrete particles in a given computational cell.

For an incompressible Newtonian fluid, the shear stress tensor $\bar{\bar{\tau}}_f$ is simply the Cauchy stress tensor with zero bulk viscosity

$$\bar{\bar{\tau}}_f = \mu_f \left[\left(\nabla \boldsymbol{u}_f + \nabla \boldsymbol{u}_f^T \right) - \frac{2}{3} \nabla \cdot \boldsymbol{u}_f \bar{\bar{I}} \right] \tag{3}$$

For the solid phase, the trajectory of the particles is obtained from the force balance given by

$$\frac{\partial \boldsymbol{u}_s}{\partial t} = \mathbf{g} \frac{(\rho_f - \rho_s)}{\rho_s} + F_D \left(\boldsymbol{u}_f - \boldsymbol{u}_s \right) + \boldsymbol{F}_{KTGF} \tag{4}$$

The terms on the right hand side of Eq.(4) are forces due to gravity, interphase drag, and particle collisions respectively. The net drag coefficient F_D is given by

$$F_D = \frac{18 \mu_f}{\rho_p d_p^2} \frac{C_D Re_p}{24} \tag{5}$$

where d_p is particle diameter, C_D is the particle drag coefficient, and Re_p is the Reynolds number based on the particle diameter, which is defined as

$$Re_p = \frac{\rho_f d_p |\boldsymbol{u}_f - \boldsymbol{u}_p|}{\mu_f} \tag{6}$$

The drag coefficient used in this work is from the drag model of Syamlal and O'Brien [16] since it corrects for the terminal velocity, which is the minimum velocity that is large enough to lift the particle out of the bed and is an important parameter for characterizing a fast fluidized bed.

$$C_D = \left(0.63 + \frac{4.8}{\sqrt{Re_p / v_{r,p}}}\right)^2 \tag{7}$$

where $v_{r,p}$ is the terminal velocity correction given by

$$v_{r,p} = 0.5(A - 0.06Re_p + \sqrt{(0.06Re_p)^2 + 0.12Re_p(2B - A) + A^2}) \tag{8}$$

$$A = \alpha_f^{4.14} \text{ and } B = \begin{cases} 0.8\alpha_f^{1.28} & \text{if } \alpha_f \leq 0.85 \\ \alpha_f^{2.65} & \text{if } \alpha_f > 0.85 \end{cases}$$

In the DDPM approach, the force due to particle collisions is computed from the particle pressure predicted by the kinetic theory of granular flows

$$\boldsymbol{F}_{KTGF} = -\boldsymbol{\nabla} \cdot \bar{\bar{\tau}}_s \tag{9}$$

2.2 Simulation of a Fast Fluidized Bed with Molochite as Bed Material

2.2.1 Geometry and Mesh

In this section, a coupled CFD/DDPM model of a fast fluidized bed is applied using molochite as the bed material. The simulation results offer an understanding of the pressure and volume fraction distribution at different heights. To simplify the simulation, the current work only considers the fuel reactor section of the Cranfield Pilot-scale Advanced Capture Technology (PACT) circulating fluidized bed reactor and maintains a constant circulating solids mass flow corresponding to the

experimental conditions by utilizing a constant solids injection. The geometry and mesh of the fuel reactor are shown in Figure 4—the geometry is a 1:1 scale model derived from the PACT reactor [17]. The riser height is 7.3 m with an inner diameter of 0.1 m, and the diameters of the particle inlet and outlet pipes are 0.04 m. The mesh is generated such that the solution is stable and converges when using a first-order numerical schemes with minimal under-relaxation to achieve faster convergence at each time step when using Fluent.

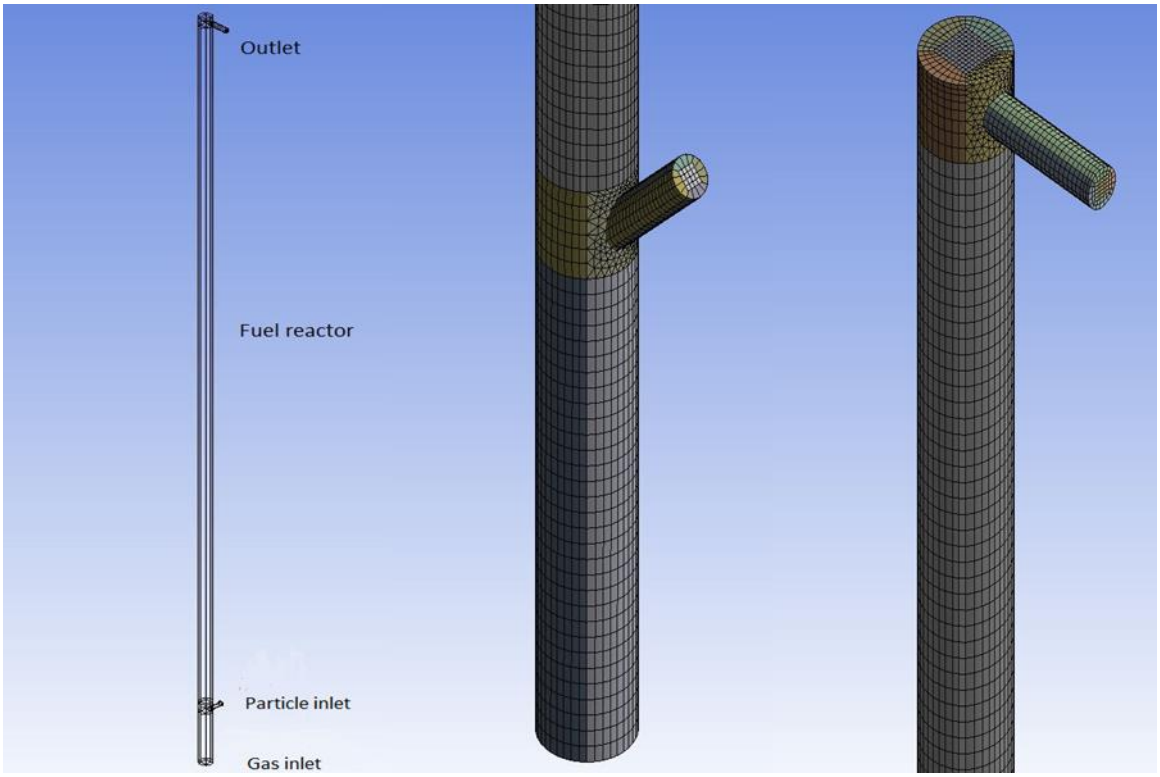

Figure 4: Geometry outline and mesh (in upper and low part) of the fuel reactor of Haider et al. [17]

2.2.2 Modeling Parameters

The molochite particles used in this simulation have a density of 1400 kg/m^3 and average diameter of 519 μm. To further reduce the computational cost, the work implements the parcel concept to simplify and accelerate the simulation process [18]. One parcel represents a cluster of particles

with the same intensive properties as the individual particles. The mass and volume of the parcels are adopted during the calculations instead of the individual particle. The parcel diameter is set at 0.002 m, which is slightly less than the minimum numerical cell size as required, so that a total of 178,265 parcels are employed initially in the entire system. The key modeling parameters used in the CFD/DDPM simulation are detailed in Table 1.

Table 1: Key modeling parameters for fast fluidized bed simulation with molochite as bed material

Particle diameter	0.000519 m
Parcel diameter	0.002 m
Particle density	1400 kg/m^3
Primary phase material	Air
Discrete phase material	Molochite
Gas inlet boundary condition	Velocity inlet at 2.55 m/s
Particle inlet boundary condition	Wall; particle injection at 3.2 kg/m^2/s
Outlet boundary condition	Pressure outlet at zero gage pressure
Drag model	Syamlal-O'Brien [16]
Numerical scheme	Phase-coupled SIMPLE
Discretization scheme	First-order upwind
Time step	Particle: 1×10^{-4} s, fluid: 1×10^{-3} s

2.2.3 Results and Analysis

The simulation is carried out on a Dell workstation using a six-core Intel Xenon CPU with ANSYS Fluent v14.5 [19, 20]. The pressure and velocity distributions are monitored at several different heights—inlet, 0.4 m, 0.45 m, 0.68 m, 0.75 m, 3.05 m, 5.0 m, 5.9 m, and 6.2 m. Prior to the start of the simulation, 178,265 particles are injected into the fuel reactor and are totally settled down for 0.5 seconds such that the kinetic energy of the particles becomes sufficiently small and the particles can be randomly distributed. This settled particle bed is considered as the initial condition for the simulation. Then, the gas inlet boundary condition is applied to inject the fluidizing gas from the bottom of the riser at a velocity of 2.55 m/s. Meanwhile, the mass flux at the particle inlet is set at 3.2 kg/m²/s, which corresponds to the solids circulation rate of Haider et al. [17]. The particle distributions and velocities are inspected at 1 s intervals and are shown in Figure 5.

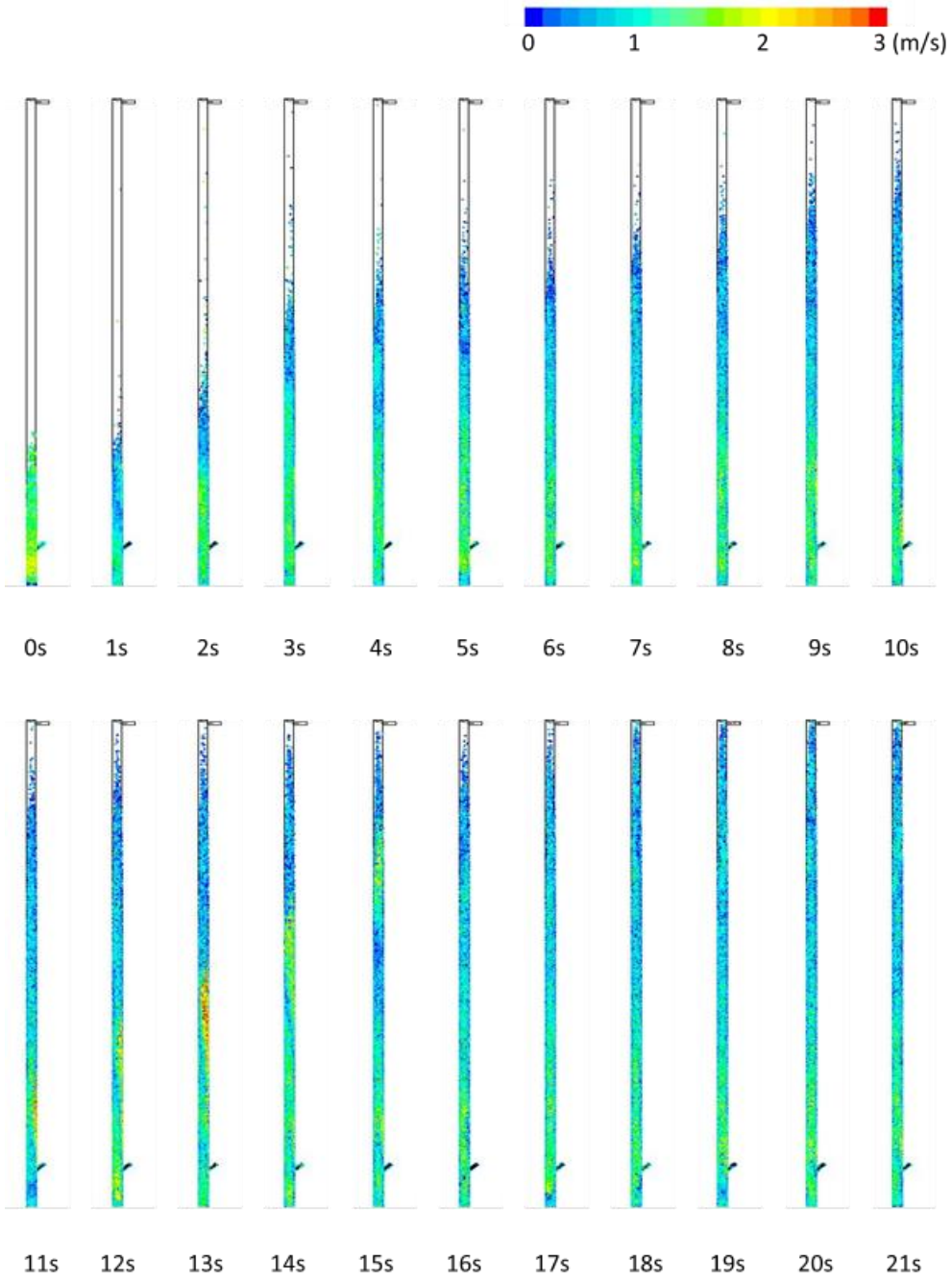

Figure 5: Particle tracks colored by velocity magnitude for the fast fluidized bed simulation with molochite

From Figure 5, the fast fluidization regime in the fuel reactor is clearly evident. Once gas is injected, the settled bed of particles experiences a sudden lift force and the particles begin to move

upward. The leading particles clusters reach the top of the reactor at around 17 s where they exit the fuel reactor (the rest of the circulating fluidized bed system is not considered in the present simulation). To further investigate the circulation condition, the particle mass flow rate at the outlet, averaged over 0.5 second intervals is shown in Figure 6.

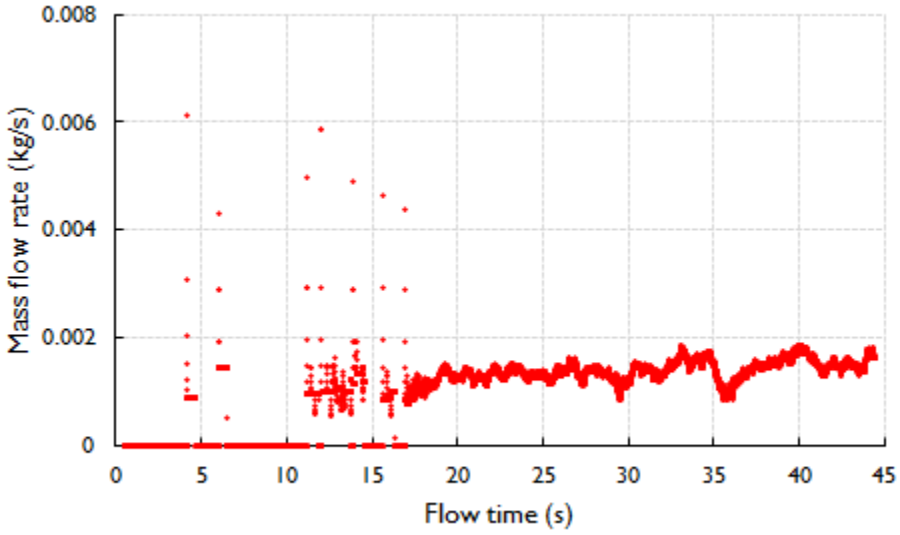

Figure 6: Time variation of outlet mass flow rate for the fast fluidized bed simulation with molochite

From Figure 6, few individual particles escape the fuel reactor from the start of the simulation at a discontinuous rate. A continuous stream of particles begins to exit the fuel reactor at around 17 s, as shown by the particle tracks in Figure 5. From this time to the end of the simulation, the mass flow at the outlet is nearly stable at around 0.002 kg/s. This is of the same order of magnitude as the particle injection rate of 0.004 kg/s used in the simulation to represent the continuous particle recirculation in the experiment of Haider et al. [17]. Hence, a stable circulating system has been

successfully achieved in this simulation. The slightly lower outlet mass flow could be explained due to a slightly reduced initial particle loading compared to the experimental condition.

Since it is the pressure gradient that drives the particles movement in the reactor, it is necessary to investigate the pressure trend. Time variation of the static pressure at 0 m (gas inlet), 0.4 m, 0.68 m, 5.9 m are shown in Figure 7. As soon as the gas is injected, it immediately experiences resistance from the settled particle bed and causes a significant spike in static pressure detected by the inlet monitor. As the gas moves through the bed, the pressure spike is still evident at different heights simultaneously but at a reduced magnitude as seen in Figure 7. With time, the particles in the bed begin to move upward by the pressure buildup leading to decrease in the pressure at the inlet and increase in higher planes. At 5.9 m from the inlet, towards the top of the bed, there is minimal effect on the pressure due to the movement of particles. The pressures in the bed stabilize after around 5 seconds when the fast fluidization regime is fully developed.

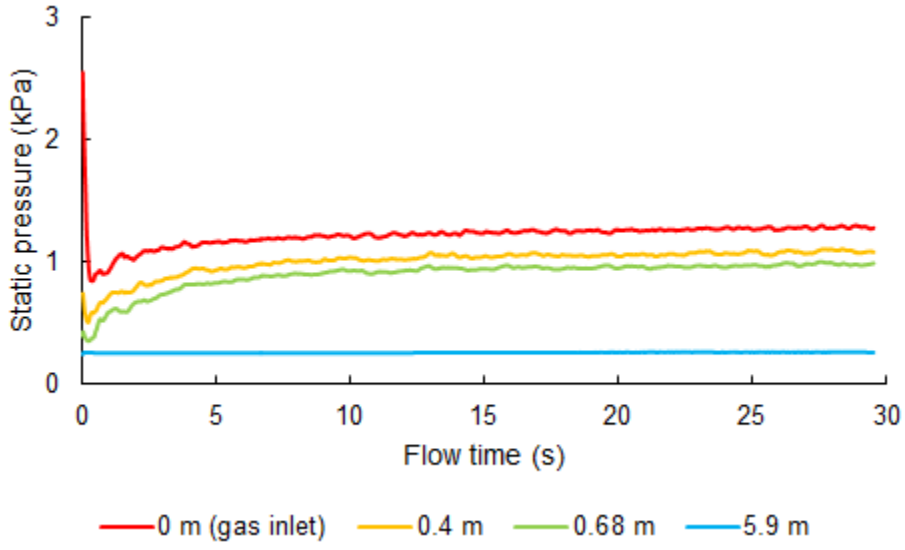

Figure 7: Time variation of static pressure at various heights for the fast fluidized bed simulation with molochite

The solids volume fractions at different heights are also investigated and shown in Figure 8. From Figure 8, from 0.5 s, the volume fraction at the bottom experiences a large change due to the gathered initial particles, and as a result of momentum transfer and particles movement, the particles at lower height are driven to the top of reactor. Higher heights of 0.4m and 0.75m experience the volume increment in the following period with a decreasing magnitude. For example, at 0.5 s, volume fraction at bottom is monitored at 0.48 and the volume fractions at 0.4m and 0.75m remain zero until 0.77 s and 1.12s, when both two planes experience a volume fraction increment of 0.2 and 0.16, respectively. Afterwards the volume fraction at various heights decreases and tends to remain unchanged after several seconds, which indicates a stable particle distribution in the reactor.

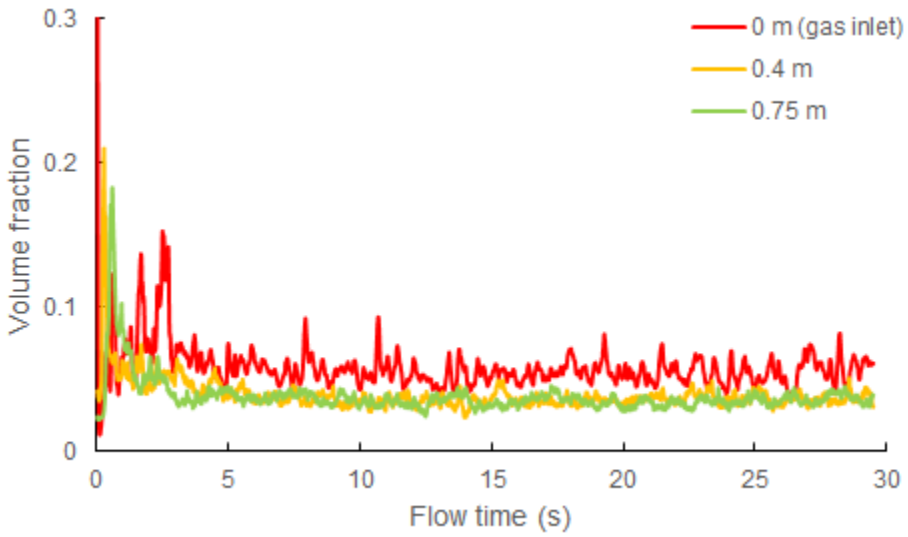

Figure 8: Time variation of volume fraction at various heights for the fast fluidized bed simulation with molochite

The captured stabilized time-averaged pressure and volume fraction along the fuel reactor are shown in Figure 9 and Figure 10 respectively and are compared with experimental data of Haider et al. [17].

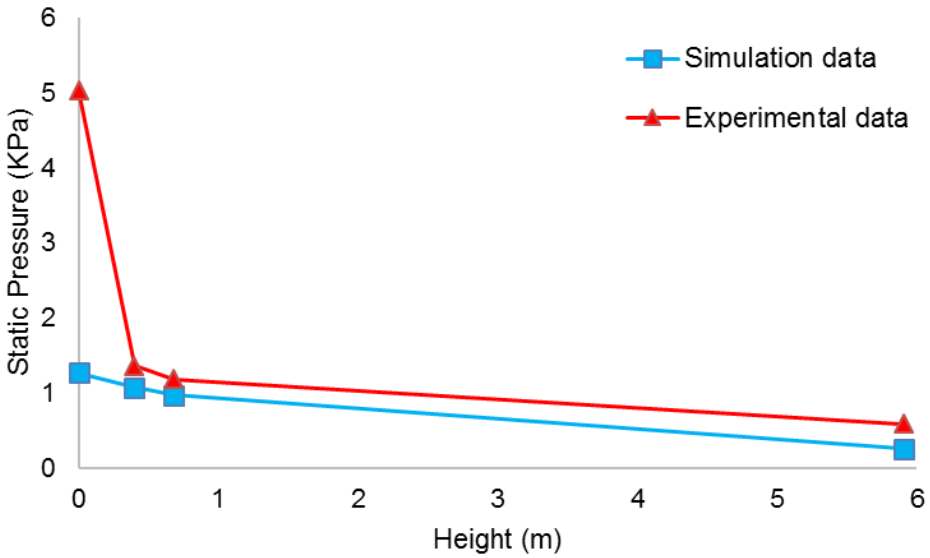

Figure 9: Comparison of pressure variation at various heights for the fast fluidized bed simulation with molochite

From Figure 9, it can be seen that the results of pressure simulation match with the experiment data both in trend and magnitude except at the bottom plane. The reason is that in the experiment, the particles are released from a narrow tunnel, while in this simulation, the particles are directly released from the bottom. This difference in the initial process leads to different initial condition at the bottom. This influence decays along the reactor and the simulation data at higher heights begins to match with the experimental results. Additionally, a pressure gradient can be observed in Figure 7, which demonstrates the crucial role the pressure plays in the circulation system.

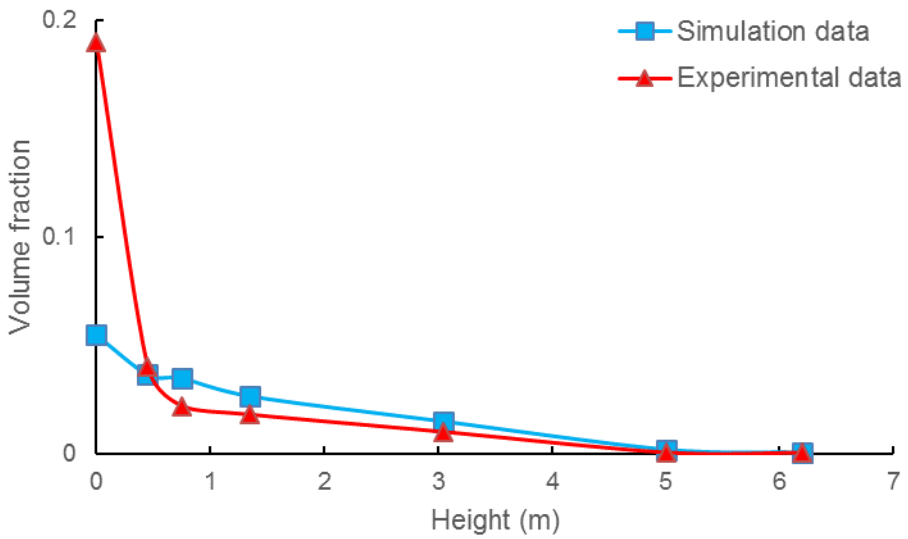

Figure 10: Comparison of volume fraction at various heights for the fast fluidized bed simulation with molochite

From Figure 10, it can be seen that the captured volume fraction at the bottom also does not match the experimental data. It is also obvious that the concentration gradient exists in the reactor, which could be considered as the major reason for pressure gradient.

In conclusion, it has been demonstrated the simulation methodology employed in this section can successfully be used for simulation of a fast fluidized bed, it is further verified in the next section by simulating a fast fluidized bed with FE100 as the bed material.

2.3 Simulation of a Fast Fluidized Bed with FE100 as Bed Material

In the previous Section 2.2, the multiphase simulations of a fast fluidized bed have shown that the CFD/DDPM can be successfully employed to determine the bed performance. In this section, a higher density bed material, FE100, is employed for simulation to provide an understanding of the effect of the material density on the performance of the fast fluidized bed.

2.3.1 Modeling Parameters

In this simulation, the bed particles are FE100 with a diameter of 6×10^{-5} m (60 μm) and a density of 5,818 kg/m³. It should be noted that although the Syamlal-O'Brien drag law [16] used in Section 2.2 works well for large diameter, low density particles like molochite, it does not provide accurate results for the fine FE100 particles considered in this section. Therefore, a more general drag law due to Gidaspow [21] is employed which is well-suited for both the packed and dilute portions of the fast fluidized bed system to capture accurately the hydrodynamic behavior. The gas injection rate is maintained at 2.55 m/s as in Section 2.2 and all other modeling parameters are shown in Table 2.

For the initialization process, 178,265 particles are released into the riser and are settled down for 500 ms. The initial conditions and particles tracks are shown in Figure 11, the velocity magnitudes indicate that most particles have low kinetic energy which is also randomly distributed. By keeping the parcel diameter same, the computational cost for this simulation is similar to the previous one using molochite.

Table 2: Key modeling parameters for fast fluidized bed simulation with FE100 as bed material

Particle diameter	6×10^{-5} m
Parcel diameter	0.002 m
Particle density	5818 kg/m^3
Primary phase material	Air
Discrete phase material	FE100
Gas inlet boundary condition	Velocity inlet at 2.55 m/s

Particle inlet boundary condition	Wall; particle injection at 3.2 kg/m²/s
Outlet boundary condition	Pressure outlet at zero gage pressure
Drag model	Gidaspow
Numerical scheme	Phase-coupled SIMPLE
Discretization scheme	First-order upwind
Time step	Particle: 1×10^{-4} s, fluid: 1×10^{-3} s

2.3.2 Results and Analysis

Similar to the previous simulation in Section 2.2, the particle distributions and velocities are inspected at 0.01 s intervals and the particle tracks and mass flow rate at the outlet are shown in Figure 11 and Figure 12, respectively.

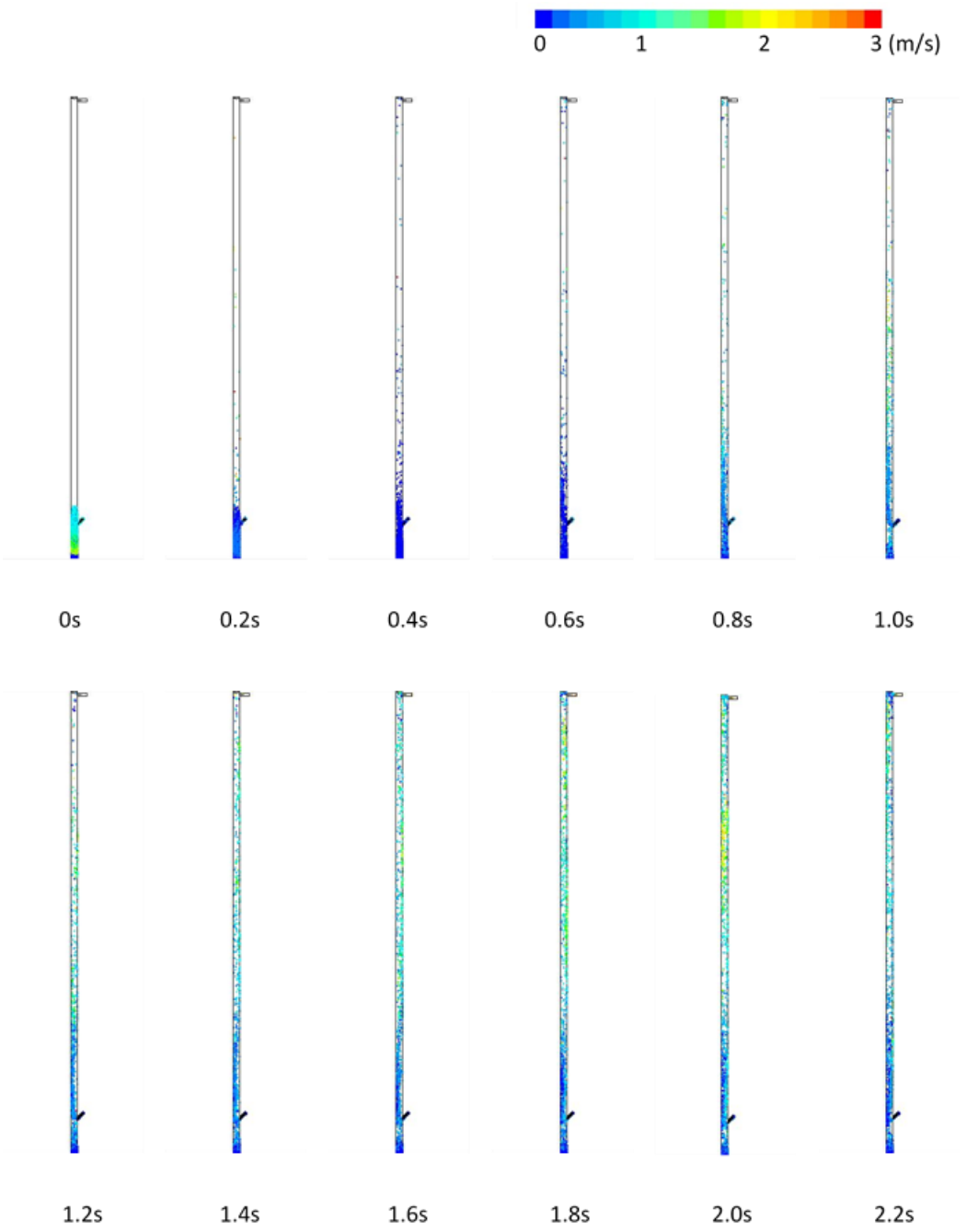

Figure 11: Particles tracks colored by velocity magnitude for the fast fluidized bed simulation with FE100

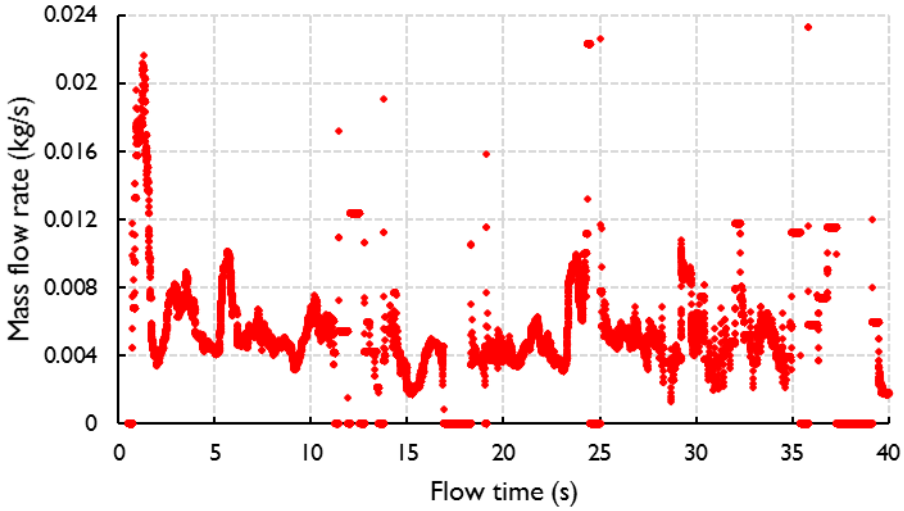

Figure 12: Time variation of outlet mass flow rate for the fast fluidized bed simulation with FE100

From Figure 11, compared to molochite, FE100 requires less time for movement and therefore the leading particle clusters reach the top of the reactor in 1.25s, it is perhaps due to decrease in the collision frequency. Because of small diameter, the FE100 particles are less likely to collide with each other when moving upward, and therefore in shorter time reach the top. One the other hand, it can be observed that the particle escape from the reactor does not show continuous behavior. The use of the Gidaspow drag law [21] in this simulation could be one possible reason, for this, although Gidaspow's drag law has shown wide applicability for various fluidized bed systems, it may not quite represent the physical behavior for the present specific situation. Thus, a further investigation into drag law is warranted. Another reason for this behavior could be the relatively coarse computation cells at the outlet; this has been a limitation of currently available computational resource. To further improve the quality of the mesh, high performance computational tool should be adopted, which will increase the computational cost. Although the

particles do not have continuous ejection from the reactor, nevertheless, the average mass flow rate from the outlet remains nearly stable from 30 s onwards, consistent with a stable circulation condition as observed in the experiment [17].

The static pressure distributions at various flow time and at different heights of the reactor are shown in Figure 13. Similar to the case in Section 2.2 with molochite as bed material, it can be seen that a pressure gradient exists in the fuel reactor. However, the pressure at the bottom of the reactor in this case experiences unsteady behavior; it is due to the irregular movement and collisions of the large number of fine FE100 particles. At higher planes, the pressure is relatively stable due to the reduced particle concentration. Particle volume fractions at various heights are shown in Figure 14. The volume fraction at the bottom of the reactor is unsteady: it increases gradually for the first 12 s and then oscillates irregularly up to 30 s, which also corresponds to the observed pressure changes in Figure 13. This is reasonable since the variation in the static pressure is caused by the presence of particles. After 30 s, the bottom volume fraction achieves relatively stable behavior. In addition, the particles behavior at the bottom only slightly affects the volume fraction at higher planes due to the small number of particles transferred.

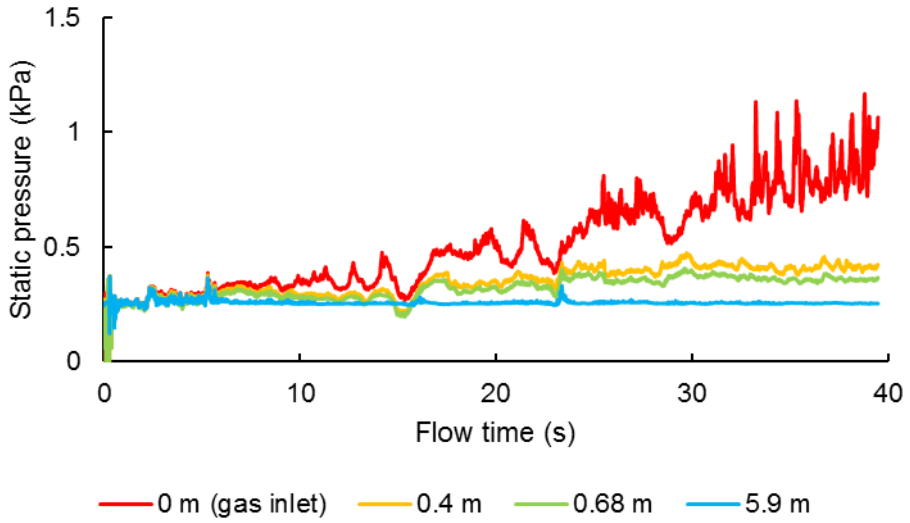

Figure 13: Time variation of static pressure at various heights for the fast fluidized bed simulation with FE100

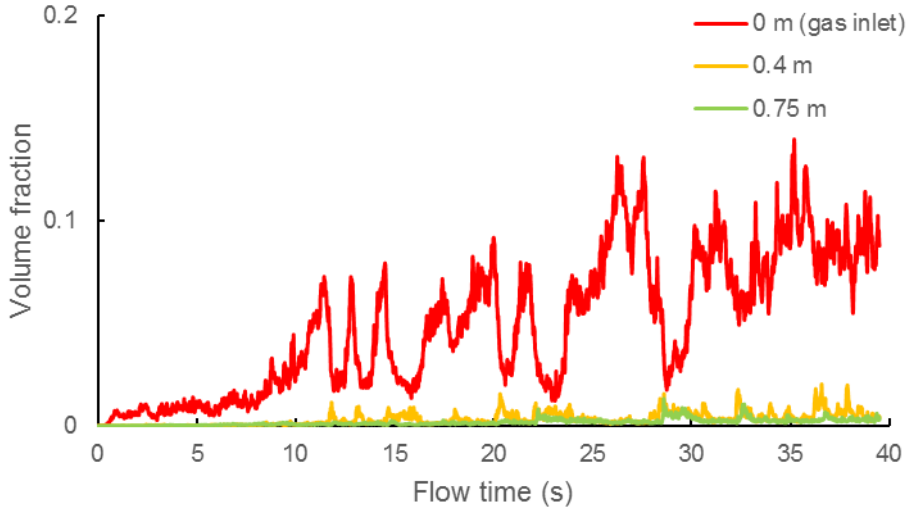

Figure 14: Time variation of volume fraction at various heights for the fast fluidized bed simulation with FE100

Comparisons of pressure and volume fraction between the simulation and experiment [17] are shown in Figure 15 and Figure 16, respectively.

From Figure 15 and Figure 16, it can be seen that the results of simulation match the experiment data reasonably well both in trend and magnitude except for differences in the inlet plane. Similar behavior was observed in the simulation with molochite in Section 2.2 and can be explained again due to the different initial processes employed in the experiment and the simulation.

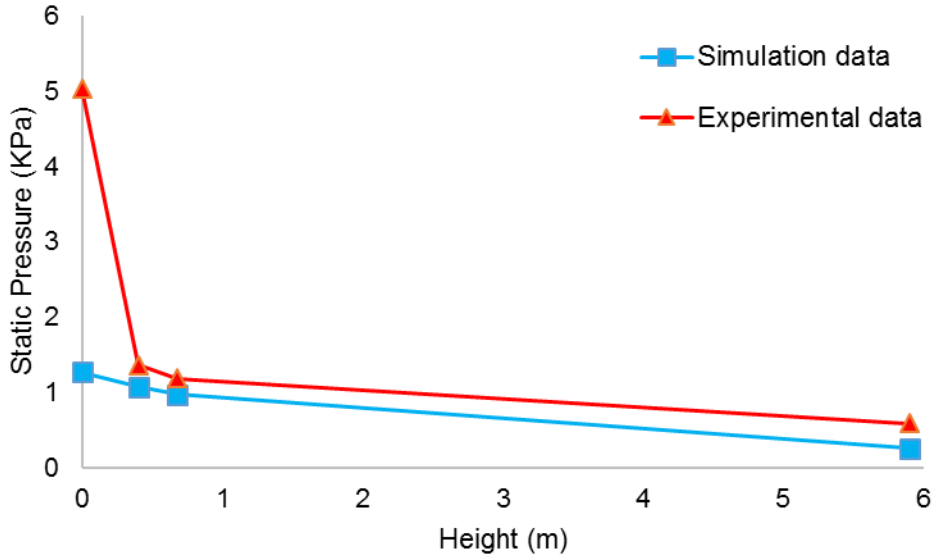

Figure 15: Comparison of pressure variation at various heights for the fast fluidized bed simulation with FE100

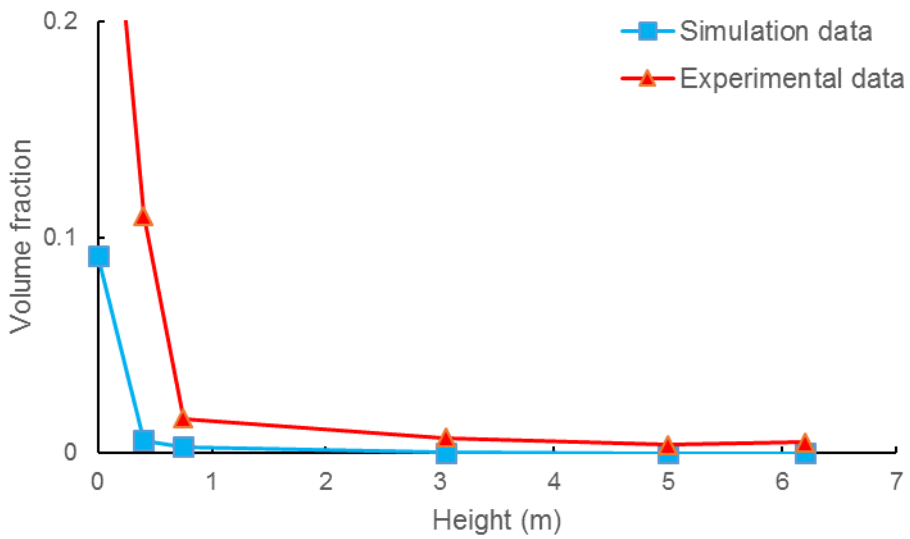

Figure 16: Comparison of volume fraction at various heights for the fast fluidized bed simulation with FE100

In spite of shortcomings in accurate description of the inlet condition and lack of continuous particle ejection from the outlet, the particles' tracks demonstrate that the fast fluidized bed setup with Gidaspow drag law employed in this section works reasonably well for high density and small diameter bed materials. The future improvements should focus on the refinement of mesh and the drag law.

2.4 Conclusion

In this chapter, CFD/DDPM multiphase cold flow simulations of a circulating fluidized bed fuel reactor have been conducted using ANSYS Fluent. The first simulation using molochite as a bed material shows good agreement with the experimental data obtained by Haider et al. [16] at Cranfield University in U.K. By employing the Syamlal-O'brien drag law, the results show that proper initial particle distribution and circulating mass flow rate in the fuel reactor are required to achieve stable circulation, and verify the variations in the static pressure and the volume fraction

inside the reactor. In order to evaluate the applicability of DDPM for high density, smaller diameter bed particles, the simulations using FE100 as bed material using the Gidaspow drag law show acceptable results compared to the experimental data. In this simulation, however the discrepancies are found, discontinuous particle ejection and unstable pressure variation at the bottom of the reactor are not observed in the experiment. There are two possibilities for those discrepancies: (1) The Gidaspow drag law may not be suitable for high density and small diameter particles and therefore does not compute the drag force accurately, and (2) the large size of computational cell may introduce errors. Nevertheless, overall these simulations demonstrate the hydrodynamic behavior of particles along the fuel reactor reasonably well and the CFD/DDPM methodology is suitable for simulation of fast fluidized beds. Future work should focus on developing a particle initialization scheme that can more accurately represent the experimental condition prior to the start of the simulation as well as improving the drag laws for various flow conditions.

Chapter 3: Transient Cold Flow Simulation of a Moving Bed in an Air Reactor

In the previous chapter, the dense discrete phase model (DDPM) showed excellent promise in simulating the fast fluidized bed of a pilot-scale fuel reactor. However, since no particle collisions are considered in dense discrete phase model, the use of DDPM is limited to dilute concentration of particles in the gas (<12%). To achieve more accurate CLC simulation with larger concentration of solid, discrete element method (DEM) would be used for better accuracy. However, it is compute intensive and therefore at present can only be employed for simulation of laboratory scale experiments.

3.1 Modeling Approach for DEM Simulation

The equations for mass and momentum conservation for the continuous phase are the same as for the dense discrete phase model given by Eqs. (1) and (2).

For the solid phase, equation is identical to Eq. (4) except for the collision force as shown in Eq. (10). The trajectory of the particles is obtained from the force balance given by

$$\frac{\partial \boldsymbol{u}_s}{\partial t} = \mathbf{g}\frac{(\rho_f - \rho_s)}{\rho_s} + F_D\left(\boldsymbol{u}_f - \boldsymbol{u}_s\right) + \boldsymbol{F}_{COL} \tag{10}$$

The collision force is computed using the soft-sphere model. The soft-sphere model decouples its normal and tangential components and the normal force in a collision, on an individual particle, it is given by

$$\boldsymbol{F}_{con}^{n} = \left(K\delta + \gamma(\boldsymbol{u}_{12}\boldsymbol{e})\right)\boldsymbol{e} \tag{11}$$

where δ stands for the overlap between the particle pair as shown in Figure 17, γ represents the damping coefficient, $\boldsymbol{e}$ is the unit vector in the direction of $\boldsymbol{u}_{12}$,which is the relative velocity of the colliding pair. In 1975, Link demonstrated the results should have no dependence on the choice of soft-sphere model and hard-sphere model for large values of K. [22], The tangential collision force is given by

$$\boldsymbol{F}_{con}^{t} = \mu \boldsymbol{F}_{con}^{n} \tag{12}$$

where μ is a function of relative tangential velocity v_r given as

$$\mu(v_r) = \begin{cases} \mu_{stick} + (\mu_{stick} - \mu_{glide})(\dfrac{v_r}{v_{glide}} - 2) & \text{if } v_r < v_{glide} \\ \mu_{glide} & \text{if } v_r \geq v_{glide} \end{cases} \tag{13}$$

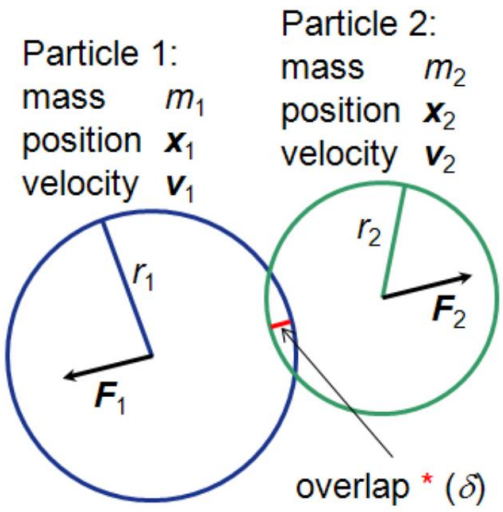

Figure 17: Schematic of particle collision model for DEM

In this chapter, Syamlal and O'Brien drag law model is again used [16] since it corrects for the terminal velocity, which is the minimum velocity that is large enough to lift the particle out of the bed and is an important parameter for characterizing a moving bed.

In addition, to predict the pressure drop of a packed bed/moving bed, Ergun equation is employed [23].

The Ergun equation gives the pressure drop across a packed/moving bed of height L as

$$\frac{\Delta p}{L} = \frac{150\mu\left(1-\alpha_g\right)^2 u_0}{{\alpha_g}^3 d_p^2} + \frac{1.75\left(1-\alpha_g\right)\rho_g {u_0}^2}{{\alpha_g}^3 d_p} \quad (14)$$

where L, α_g, d_p, u_0, ρ_g represent the height of the bed, porosity, particle diameter, superficial velocity and gas density, respectively.

3.2 Simulation of Cross Flow Moving Fluidized Bed with Iron as Bed Material

In this section, a coupled CFD/DEM model of a cross flow moving bed of the novel iG-CLC air reactor is developed with low grade iron as the bed material. The simulation results offer an understanding of the pressure drop and particle velocity distribution at different heights of the bed. The iG-CLC industrial-scale experiment was conducted by Wang et al. at Southeast University [24].

3.2.1 Geometry and Mesh

The geometry and mesh of the air reactor are shown in Figure 18 and Figure 19. To reduce the computational cost during the simulation, the geometry is a 0.5:1 scale model derived from the novel iG-CLC experimental system. The cuboid-shaped air reactor is 1 meter in height, and the channel of moving bed is 700mm in height, 100mm in width, and 100mm in depth. The angle, length and spacing of louver are 75°,130mm, and 60mm, respectively. The mesh is generated as that the solution is stable when using a first-order numerical schemes with minimal under-relaxation to achieve faster convergence at each time step.

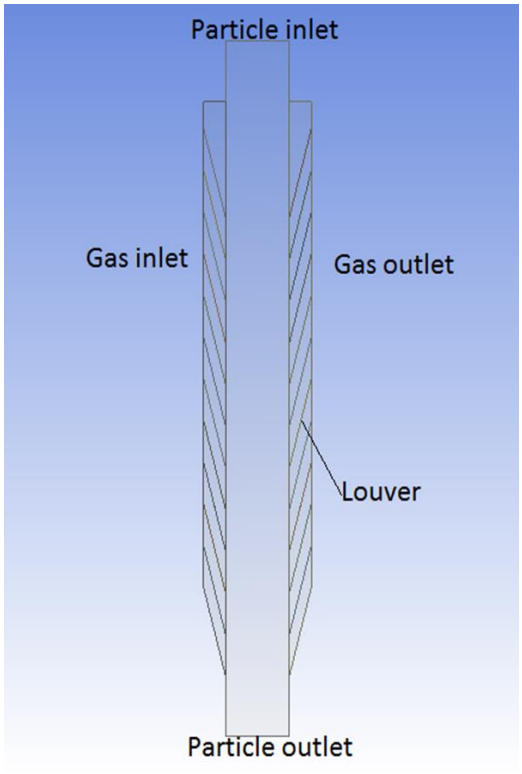

Figure 18: Geometry outline of the air reactor of Wang et al. [24]

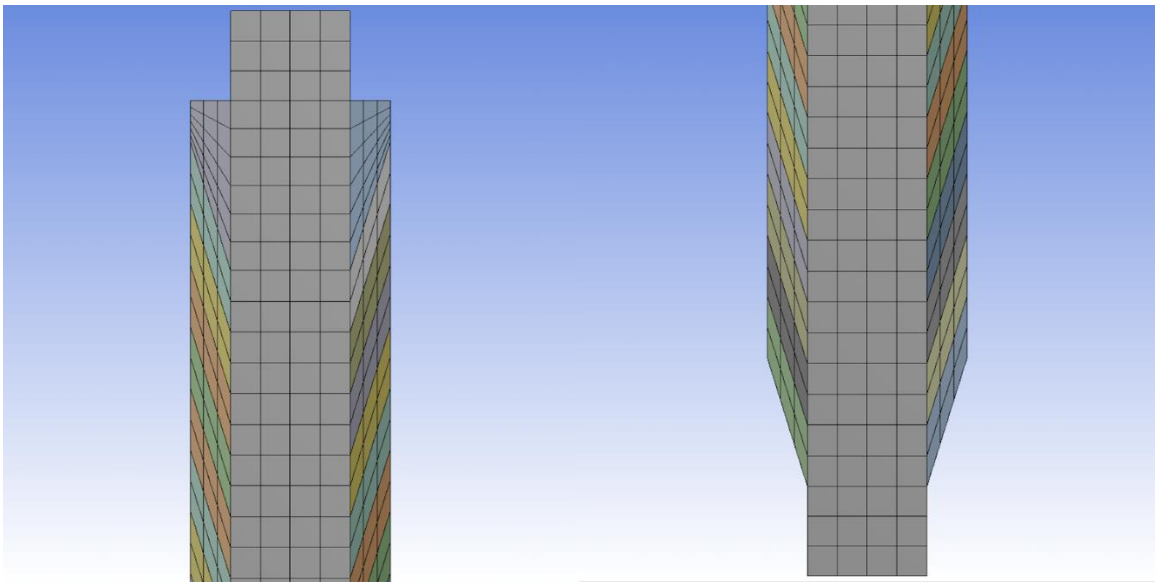

Figure 19: Mesh (in upper and lower part) of the air reactor of Wang et al. [24]

3.2.2 Modeling Parameters

The low-grade iron particles used in this simulation have a density of 3505 kg/m^3 and average diameter of 710 μm. To further reduce the computational cost, the parcel concept is implemented. The parcel diameter is set at 0.002 m, which is slightly less than the minimum numerical cell size as required. The minimum fluidization gas velocity is 0.45 m/s. Different from previous DDPM simulation, this cross flow moving bed does not have pre-installed particles. Particles are injected from the top particle inlet at a constant mass flow rate of 4.4kg/m^2/s. The gas is injected from the gas inlet at a horizontal velocity of 0.00489 m/s and vertical velocity of -0.01826 m/s, which is obtained from the fluidizing number. The fluidizing number is defined as the ratio between the superficial gas velocity and the minimum fluidizing velocity of the bed materials. The boundary conditions at gas inlet and gas outlet are velocity inlet and pressure outlet, respectively. The boundary conditions at particle inlet and particle outlet are walls where DPM particles are injected and escape, respectively. The key modeling parameters used in the CFD/DEM simulation are given in Table 3.

Table 3: Key modeling parameters for moving bed simulation with iron as bed material

Particle diameter	7.1×10^{-4} m
Parcel diameter	0.002 m
Particle density	3505 kg/m^3
Primary phase material	Air
Discrete phase material	Iron
Gas inlet boundary condition	Horizontal velocity at 0.00489 m/s Vertical velocity at -0.01826 m/s
Particle inlet boundary condition	Wall; particle injection at 4.4 kg/m²/s
Outlet boundary condition	Pressure outlet at zero gage pressure
Drag model	Syamlal-O'Brien
Numerical scheme	Phase-coupled SIMPLE
Discretization scheme	First-order upwind
Time step	Particle: 1×10^{-5} s, fluid: 1×10^{-4} s

3.2.3 Results and Analysis

The simulation is carried out on a Dell workstation using a six-core Intel Xenon CPU with ANSYS Fluent v14.5. The total simulation takes up about 0.5 s. The total pressure distributions are monitored at gas inlet and gas outlet. The particles distribution is inspected at 2 ms intervals and are presented in Figure 20.

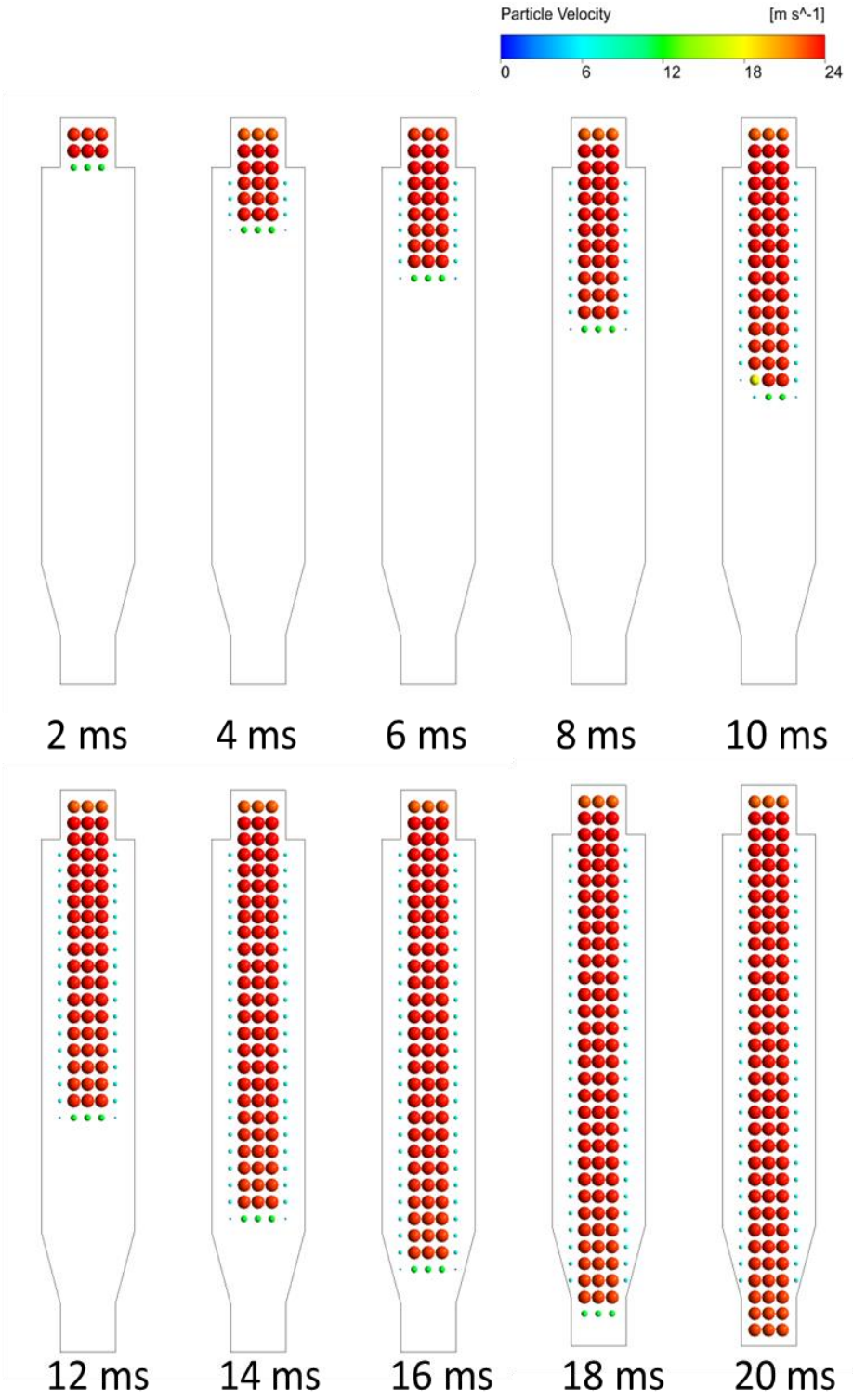

Figure 20：Particle tracks colored by velocity magnitude for the moving bed simulation with iron

From Figure 20, the moving bed regime in the air reactor is evident. Once particles are injected, they move downward towards the particle outlet, the gas injection slightly changes the horizontal velocity due to its small value but accelerates the falling particles. The leading particles cluster reaches the bottom of the reactor at around 20 ms. The pressure distributions and their difference are shown in Figure 21.

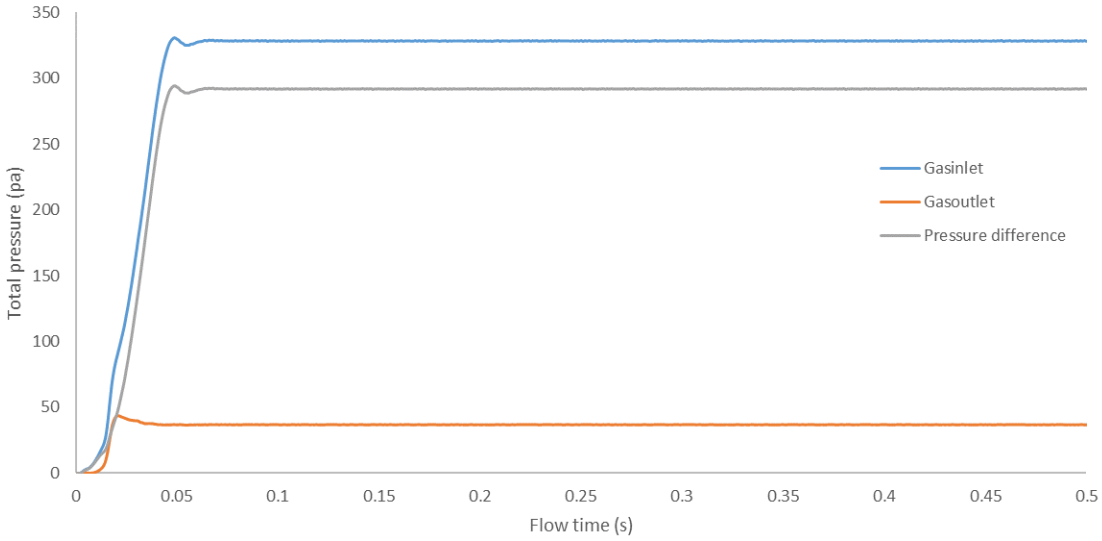

Figure 21: Time variation of total pressure for the moving bed simulation with iron

From Figure 21, it can be seen that the area-averaged total pressure at the gas inlet is larger than that at the gas outlet, which implies that a horizontal pressure gradient is generated to induce the particles cluster to get fluidized. Also, the total pressure becomes stable after 0.05s, which indicates that a stable circulation is achieved. The total pressure difference has the same shape as the pressure at gas inlet and gas outlet, as expected. The total pressure difference also becomes stable at 0.02m, and the average total pressure difference is 291 pascal. According to Ergun equation, once the bed material and superficial velocity is fixed, the pressure gradient is also fixed. The scaled experimental pressure drop is 389 pascal [24]. Thus the simulation pressure drop has a

reasonable good agreement with the experimental result. This clearly demonstrates that the cross flow moving bed setup employed here is a good choice.

To determine the particle velocity distribution in various planes of the moving bed, four monitors at 0.1m,0.2m,0.3m,0.4m bed height are employed as shown in shown as Figure 22.

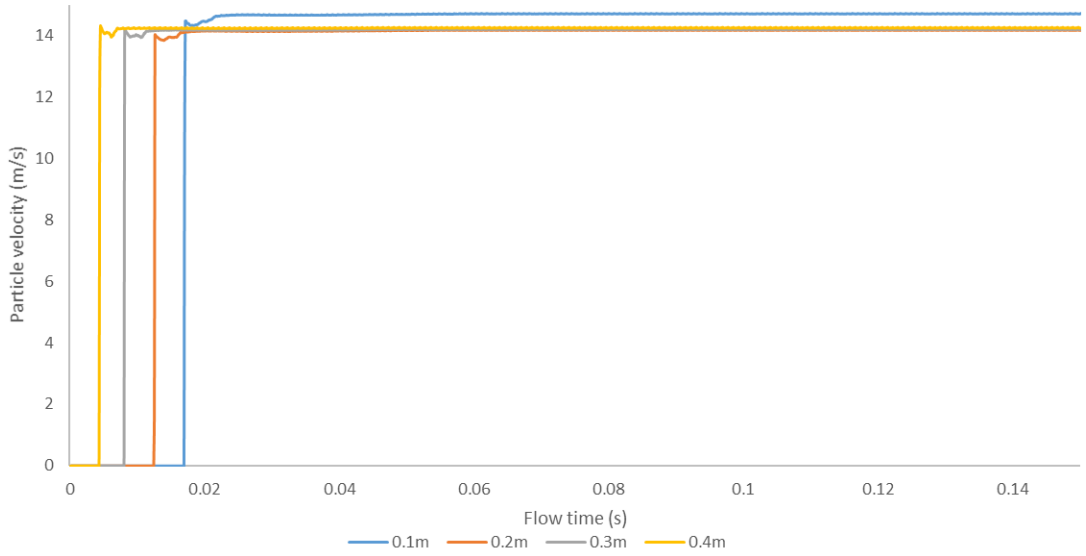

Figure 22: Time variation of particle velocity at various heights for the moving bed simulation with iron

In Figure 22, the monitored planes detect area-averaged particle velocity. All particles besides lower plane particles attain the same velocity; This demonstrates that a stable moving bed regime has fully developed in the air reactor. The reason for slightly higher particle velocity at the low plane is the change of cross section area. At the lower plane, in order to connect the downcomer, the channel begins to shrink, due to the conservation of mass, the particle velocity will correspondly increase. More details of the stabilized velocity distributions are shown in Figure 23.

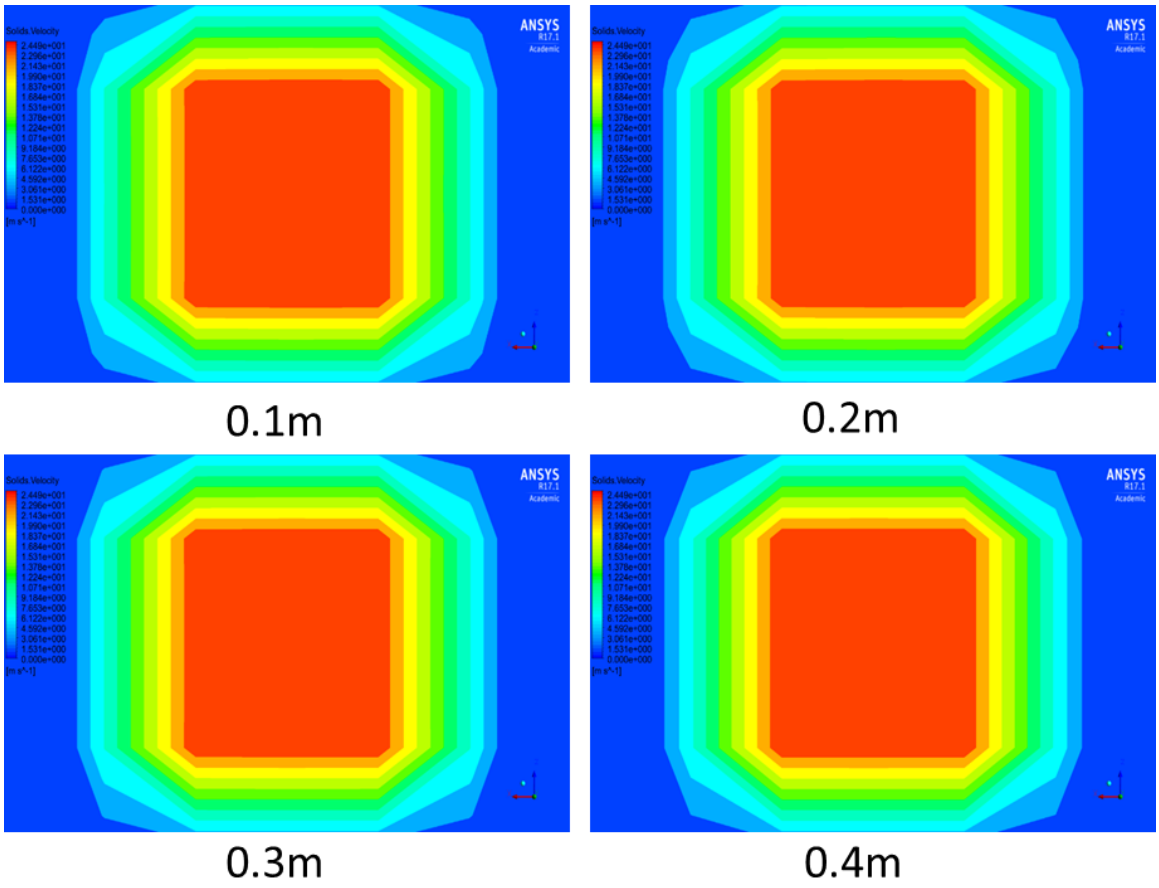

Figure 23: Fully developed particle velocity distribution at various heights for the moving bed simulation with iron

From Figure 23, it can be seen that once the cross flow moving bed regime has fully developed, particle velocity distributions at different heights remain unchanged except for lower plane, the reason has been explained above. At this condition, the gravitational force is balanced by the drag force, particles move with identical velocities towards the outlet, which is exactly the behavior of a moving bed.

Since the flow pattern largely influences the movement of the particles, the flow field inside the reactor is also of interest. The development of internal flow is shown as Figure 24.

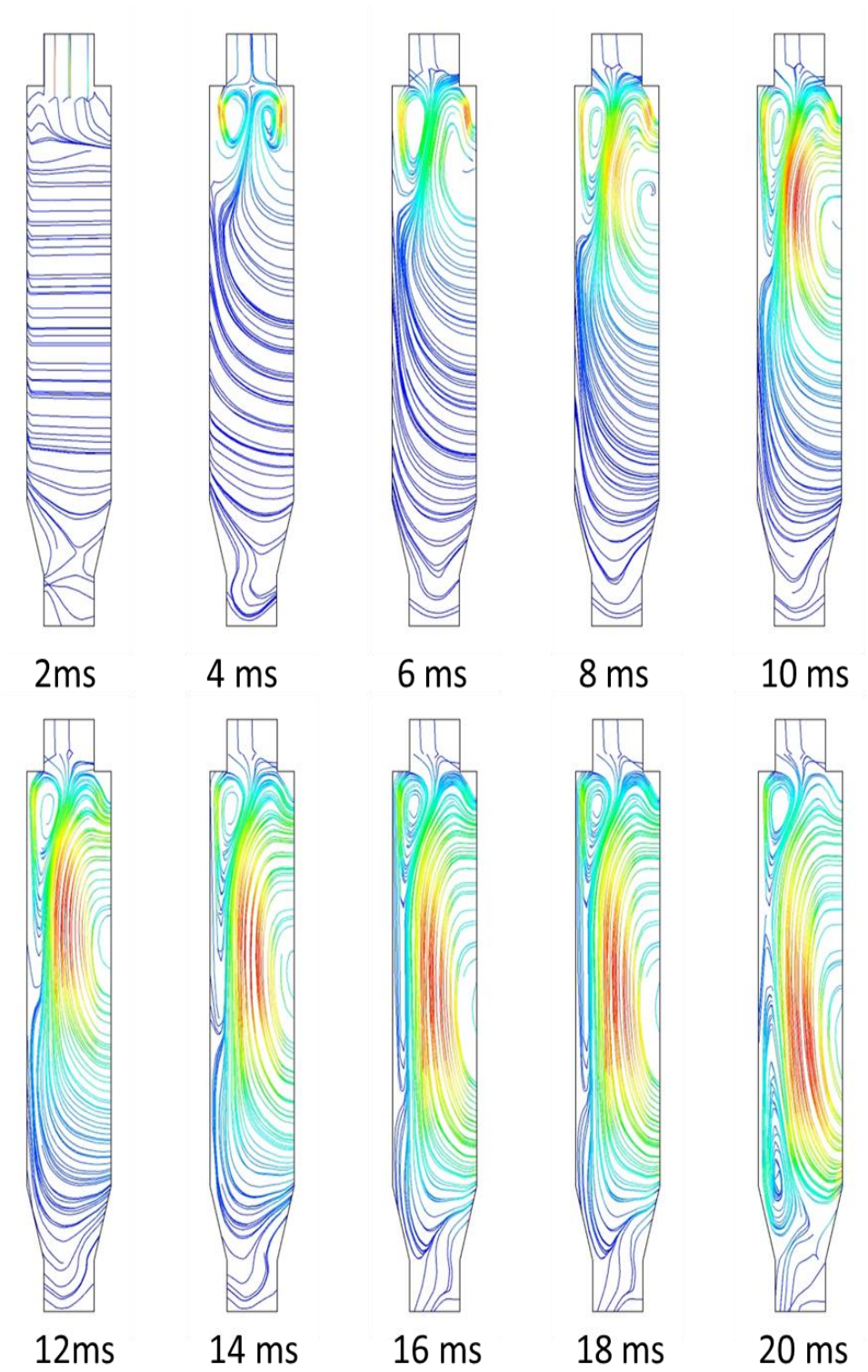

Figure 24: Developing flow field streamlines for the moving bed simulation with iron

From Figure 24, as particles move towards outlet, the flow field changes gradually, and vortex are generated due to difference of pressure gradient. Once the flow stabilizes, a dual-vortex pattern occurs inside the reactor. The gas injected from left gas inlet moves downward at an angle of 75° before it encounters the particle wall. Then the gas moves downward, and gas gradually decreases in velocity and finally switches direction to move upward. A vortex is formed when the gas reaches the top boundary and finally the injected gas escapes from the reactor through the right gas outlet. At the right side of the air reactor, due to pressure difference between the top and the bottom boundary, reversible flow is generated on the top part of the gas outlet and this gas flow moves directly towards the bottom part of the gas outlet generating another recirculation. This flow pattern also explains the nearly constant velocity of the particles in the central parts.

3.2.4 Conclusion

In this chapter, CFD/DEM multiphase cold flow simulations of a cross flow moving bed have been conducted by using ANSYS Fluent. By using iron as bed material, simulations show excellent agreement with the experimental data of Wang et.al obtained at Southeast University. By employing the Syamlal-O'Brien drag law, the results show that the injection particles and gas injection velocity chosen are proper to achieve a stable circulation and the simulation successfully captures the moving bed behavior. In addition, a dual-vortex pattern is formed during the process and makes significance to the formation of moving bed regime. This simulation demonstrates the hydrodynamic behavior of particles in the air reactor and verifies that the CFD/DEM model is an appropriate method for animation of industrial scale moving bed.

Chapter 4: Conclusion and Future Work

In this thesis, CFD simulations of a fast fluidized bed of a dual circulation CLC system and a cross flow moving bed in an air reactor have been successfully conducted. In the first fast fluidized bed simulations, velocity and pressure distribution are compared with experimental results, and it is shown that the simulations have achieved excellent agreement with experiment. The current work provide insight in 3-D simulation of CLC process and the importance of pressure field inside the reactor. In the moving bed simulation, the total pressure difference is compared between simulation and experiment, also a satisfactory result is obtained. And the moving bed behavior is captured. A dual-vortex pattern formation is analyzed and velocity distribution in the air reactor is observed. This work demonstrates the significance of studying flow pattern hydrodynamics behavior of particles inside an air reactor.

Even though successful simulation results have been obtained in this thesis, there are many improvements that should be considered in the future work. First, the geometry of the CLC reactor plays an important role in the performance of a CLC system. The entire geometry of the CLC system, including the fuel and air reactors should be modeled with a very fine mesh; A larger number of particles should be used in both DDPM and DEM simulation by using more powerful computers. Improved drag laws and particle collision models should be developed. Hot flow simulations with chemical reactions should be performed.

References

[1] S. Arrhenius, "On the influence of carbonic acid in the air upon the temperature of the ground," *Philosophical Magazine and Journal of Science,* vol. 41, pp. 237-276, 1896.

[2] A. Epstein, Moral case for fossil fuel, New York: Penguin Group (USA) LLC, 2014.

[3] U. E. I. Adminstration., "International Energy Outlook 2010," U.S. Department of Energy, Washington, DC, 2010.

[4] A. Lyngfelt and B. Leckbner, "Minisymposium in CO2 capture and storge," in *Technologies for CO2 separation*, Gothenburg, Sweden, 1999.

[5] T. Mattisson and A. Lyngfelt, "Capture of CO2 using chemical-looping combustion," in *First Biennial Meeting of the Scandinavian-Nodic Section of the Combustion Institute*, Goteborg, Sweden, 2001.

[6] S. Banerjee and R. K. Agarwal, "Transient reacting flow simulation of spouted fluidized bed for coal-direct chemical looping combustion with different Fe-based oxygen carriers," *Applied Energy,* vol. 160, pp. 553-560, 2015.

[7] N. V. Gnanapragasam, B. V. Reddy and M. A. Rosen, "Hydrogen production from coal using coal direct chemical looping and syngas chemical looping combustion systems: assessment of system operation and resource requirements," *Hydrogen Energy,* vol. 34, no. 6, pp. 2606-2615, 2009.

[8] D.Geldart, "Types of gas fluidization," *Powder Technology,* vol. 7, pp. 285-292, 1973.

[9] J. Jung and I. K. Gamwo, "Multiphase CFD-based models for chemical looping combustion process: Fuel reactor modeling.," *Powder Technology,* vol. 183, no. 3, pp. 401-409, 2008.

[10] J. Ding and D. Gidaspow, "A bubbling fluidization model using kinetic theory of granular flow," *AIChE,* vol. 36, no. 4, pp. 523-538, 1990.

[11] A. Almstedt and H. Enwald, "Fluid dynamics of a pressurized fluidized bed: comparison between numerical solutions from two-fluid models and experimental results," *Chemical Engineering Science,* vol. 54, no. 3, pp. 329-342, 1999.

[12] J. Ghaboussi and R. Barbosa, "Three-dimensional discrete element method for granular materials," *Numerical and Analytical Methods in Geomechanics,* vol. 14, no. 7, pp. 451-472, 1990.

[13] S. Cloete, S. Johansen and M. B.Popoff, "Evaluation of a Lanrangian Discrete Phase Modeling approach for resolving cluster formation in CFB risers," in *International Conference on Multiphase Flow*, Leipzig,Germany, 2010.

[14] X. Chen and J. Wang, "A comparison of Two-fluid model, dense discrete particle model and CFD-DEM method for modeling impinging gas-solid flows," *Powder Technology,* vol. 254, pp. 94-102, 2014.

[15] ANSYS, ANSYS FLUENT Theory Guide, Canonsburg, PA, 2012.

[16] M. Syamlal and T. O'Brien, "Computer simulation of bubbles in a fluidized bed," *AIChe Symposium series,* vol. 85, pp. 22-31, 1989.

[17] S. K. Haider, L. Duan, K. Patchigolla and E. Anthony, "A hydrodynamic study of a fast-bed dual circulating fluidized bed for chemical looping combustion," *Energy Technology,* vol. 4, no. 10, pp. 1254-1262, 2016.

[18] N. Patankar and D. Joseph, "Modeling and numerical simulation of particulate flows by the Eulerian-Langrangian approach," *Multiphase Flow,* vol. 27, no. 10, pp. 1659-1684, 2001.

[19] ANSYS, "ANSYS Fluent User's Guide," ANSYS, Inc., Canonsburg, PA, 2012.

[20] ANSYS, "ANSYS Fluent Theory Guide," ANSYS, Inc., Canonsburg, PA, 2012.

[21] D. Gidaspow, Multiphase Flow and Fluidization, San Diego,CA: Academic Press, 1992.

[22] J. M. Link, "Development and validation of a discrete particle model of a spout-fluid bed granulator," Phd dissertation, University of Twente, Enschede, The Netherlands, 1975.

[23] S. Ergun, "Fluid flow through packed columns," *Chem.Eng.Prog.Symp.Ser.,* vol. 62, pp. 100-111, 1966.

[24] X. Wang, B. Jin, X. Liu, Y. Zhang and H. Liu, "Experimental Investigation on flow behaviors in a novel in situ gasification chemical looping combustion apparatus," *Industrial & Engineering Chemistry Research,* vol. 52, pp. 14208-14218, 2013.

[25] J. Yerushalmi, D. H. Turner and A. M. Squires, "The fast fluidized bed," *Industrial & Energineering Chemistry Research,* vol. 15, pp. 47-53, 1976.

[26] L. Zou, Y. Guo and C. Chan, "Cluster-based drag coefficient model for simulating gas-solid flow in a fast fluidized bed," *Chemical Engineering Science*, vol. 63, no. 4, pp. 1052-1061, 2008.

Curriculum Vita

Mengqiao Yang

Degrees

M.S., Mechanical Engineering, Washington University in St. Louis, May 2017

B.Eng., Building Environment and Energy Application Engineering (City Gas), Jilin Jianzhu University, June 2015

Publications

Mengqiao Yang, Subhodeep Banerjee, Ramesh Agarwal. Transient Cold Flow Simulation of Fast Fluidized Bed Fuel Reactors for Chemical Looping Combustion[J]. Journal of Energy Resources and Technology (Under Review)

Mengqiao Yang, Li Bai. Research Status of Natural Gas Leak Detection Technology [J]. Gas & Heat, 2014, 34(10): B11-B14.

Shimei Sun, Xinyu Zhang, **Mengqiao Yang**. Lithium ion battery efficient thermal management numerical simulation [C], Applied Mechanics and Materials, 2014(672-674):646-651.

Shimei Sun, Xinyu Zhang, **Mengqiao Yang**. Lithium ion battery temperature field numerical simulation [C], Applied Mechanics and Materials, 2014(672-674):652-656.

Shurui Li, Li Bai, **Mengqiao Yang**. Analysis of Soil Heat Balance for GSHP System[J], Journal of Jilin Institute of Architecture & Civil Engineering, 2014,31(4):33-36.

This page is intentionally left blank